




Effects of neutron-skin thickness on light-particle production

Meng-Qi Ding (丁梦琦) ¹, De-Qing Fang (方德清) ^{1,2,*} and Yu-Gang Ma (马余刚) ^{1,2,†}

¹Key Laboratory of Nuclear Physics and Ion-beam Application (MOE), Fudan University, Shanghai 200433, China

²Shanghai Research Center for Theoretical Nuclear Physics, NSFC and Fudan University, Shanghai 200438, China



(Received 10 September 2023; accepted 19 January 2024; published 26 February 2024)

Within the framework of the isospin-dependent quantum molecular dynamics (IQMD) model, we simulate the semiperipheral collisions of neutron-rich Ca, Mg, and Ne isotopes on ^{12}C target at 50 MeV/nucleon. Different neutron-skin thicknesses (S_n) of projectiles are obtained by adjusting the neutron diffuseness parameter in the droplet model. It is suggested that in both initial and final states, the difference of momentum between neutrons and protons [$\Delta P(n-p)$] decreases linearly with the increase of S_n . The similar correlation exists between S_n and the peak position of the momentum spectrum of neutrons (g_1). Moreover, the yield ratio of neutrons to protons [$R(n/p)$] is proportional to S_n and $R(n/p)$ with lower momentum is more sensitive to S_n . The above analyses are also applied to the triton and ^3He , which displays some limitations of their dependence on S_n . Therefore, $\Delta P(n-p)$, g_1 , and $R(n/p)$ can be taken as general experimental observables to extract information on S_n .

DOI: [10.1103/PhysRevC.109.024616](https://doi.org/10.1103/PhysRevC.109.024616)

I. INTRODUCTION

The density distribution is one of the fundamental properties of nuclei which is related to the single particle orbit and wave function of the nuclei. With the development of radioactive beam physics, the study interest on nuclei far away from the β -stability line has been greatly increased and a series of new physical phenomena have been discovered, such as new magic numbers, collective motion modes, and exotic structures [1–4]. Especially, the structure of neutron skin or halo is one of the most important properties in exotic nuclei. For the neutron-rich nucleus, with neutron number (N) larger than proton number (Z), the excess neutrons tend to be on the surface of the nucleus, thus forming a neutron-rich region which is called the neutron skin. The neutron-skin thickness is defined as the difference between the root-mean-square (rms) radii of neutron and proton density distributions: $S_n \equiv \langle r_n^2 \rangle^{1/2} - \langle r_p^2 \rangle^{1/2}$. The radius of the proton density distribution can be measured with high accuracy by electromagnetic interaction [5], but it is a challenge to obtain the precise radius of the neutron density distribution directly in experiments because of its charge neutrality. So far, there are various experimental methods to measure the distribution of neutron by strong or weak interaction probes, such as hadron scattering [6,7], giant dipole resonance (GDR) [8,9], spin dipole resonance (SDR) [10], and antiprotonic annihilation [11,12]. However, the deduced results change significantly with experimental analysis methods and have much lower experimental accuracy compared with the proton radius [13]. Therefore, further investigations on observable of neutron-skin thickness is expected, which is of great importance in nuclear physics and astrophysics.

The equation of state (EOS) of nuclear matter is one of the key problems in nuclear physics, which reflects the interaction between microscopic particles in a macroscopic viewpoint [1,14–16,16–25]. Previous studies have found that there is a direct correlation between the neutron-skin thickness of the neutron-rich nucleus and the symmetry energy term in the EOS of nuclear matter [26–34], thus providing the possibility of obtaining information on the symmetry energy and determining the form of the EOS. For example, with the help of the Skyrme-Hartree-Fock (SHF) [26] and some other models [33], it has been demonstrated that there is a strong linear correlation between the neutron-skin thickness and the slope of the symmetry energy at the saturation density for the heavy nucleus ^{208}Pb . Furthermore, it is of great significance in understanding the properties of neutron stars and other compact objects in nuclear astrophysics. Some properties of neutron stars depend on the EOS, including the crust-to-core transition, the cooling, and the relationship between the mass and radius, as a result of which we can give some constraints on the properties of neutron stars by extracting the nuclear EOS from experimental measurements in nuclear physics [18,27–29,31,35–40].

It is known from quantum mechanics that the wave function in the coordinate representation and momentum representation are Fourier transforms. Besides, Heisenberg proposed the uncertainty principle between position and momentum, expressed as $\sigma_x \sigma_p \geq \hbar/2$, where σ_x and σ_p are the uncertainty of position and momentum, respectively. It implies that we cannot determine the position and momentum of a particle precisely at the same time. Because it is easier to measure the momentum than the density distribution for neutrons in experiments, it may be interesting to study the dependence of the difference of momentum between neutrons and protons with neutron-skin thickness.

Besides, based on the isospin-dependent quantum molecular dynamics (IQMD) model with different neutron density

*dqfang@fudan.edu.cn

†mayugang@fudan.edu.cn

distributions for the initialized projectile, Refs. [41,42] found that the yield ratio of neutrons to protons [$R(n/p)$] is proportional to the neutron-skin thickness. However, according to the problem of efficiency of detecting neutrons in experiments, Ref. [43] proposed that the yield ratio of tritons to ^3He [$R(t/^3\text{He})$] could be taken as a more effective experimental observable to extract the neutron-skin thickness. Recently, Refs. [44,45] have further proved the above conclusions. Additionally, by using the isospin-dependent Boltzmann-Uehling-Uhlenbeck (IBUU) transport model [14,46–48], Ref. [49] indicated that $R(n/p)$ as a function of their kinetic energies is affected significantly by the density dependence of the nuclear symmetry energy. Similarly, Ref. [50] manifested that both the yields and energy spectra of light clusters (deuteron, triton, and ^3He) are sensitive to nuclear symmetry energy. It is found that a softer symmetry energy gives a smaller yield of these clusters and this effect is large when they have lower kinetic energies. It is worth noting that the nuclei involved in the above studies are all heavy, such as Ca with mass number larger than 48, Ni, and Sn. It would be also valuable to investigate the reactions at around 50 MeV/nucleon with lighter neutron-rich nuclei as projectiles, like Mg isotopes, which could be measured at the heavy-ion research facility in Lanzhou (HIRFL).

In the present paper, we employ the IQMD model to simulate heavy-ion collisions induced by neutron-rich nuclei at intermediate energies and explore the correlation between the neutron-skin thickness and some physical quantities of the emitted light particles (neutron, proton, triton, and ^3He), such as the momentum difference, momentum spectrum, and yield ratio. The sensitivities of several probes of neutron-skin thickness will be further investigated.

II. MODEL AND METHOD

The quantum molecular dynamics (QMD) model is a semi-classical microscopic transport theory to describe heavy-ion collisions from intermediate to relativistic energies which has been extensively and successfully used [47,48,51–63]. It involves three basic elements: the mean field, two-body nucleon-nucleon collision, and Pauli blocking, giving us detailed phase space information of nucleons and fragments. With the advance of radioactive beam physics, the isospin degree of freedom plays a crucial role in explaining certain physical phenomena, and the isospin-dependent interaction is therefore introduced into the QMD model simulation, which is called an isospin-dependent QMD (IQMD) [55,64]. In the IQMD model, instead of a classical point particle, each nucleon is regarded as a Gaussian wave packet with finite width in both coordinate space and momentum space, expressed as

$$\phi_i(\vec{r}, t) = \frac{1}{(2\pi L)^{3/4}} \exp\left[-\frac{[\vec{r} - \vec{r}_i(t)]^2}{4L} + \frac{i\vec{r} \cdot \vec{P}_i(t)}{\hbar}\right], \quad (1)$$

where $\vec{r}_i(t)$ and $\vec{P}_i(t)$ are the spatial center and momentum center of the i th wave packet, respectively, and L is the square of the width of the wave packet, which is set to be 2.16 fm^2 in our study [64–66]. Then the wave function of the whole system is a direct product of coherent state $\phi_i(\vec{r}, t)$. The initial

values of the phase space parameters $\vec{r}_i(t)$ and $\vec{P}_i(t)$ are given by the Monte Carlo sampling. The coordinate of the nucleon can be sampled from a given density distribution and the Fermi momentum is calculated by

$$P_F^i(\vec{r}) = \hbar[3\pi^2 \rho_i(\vec{r})]^{1/3}, \quad i = n, p \quad (2)$$

to obtain the momentum of the nucleon by the random sampling from $[0, P_F^i]$. The evolution of every single nucleon follows the Hamilton canonical equation. The effective potential U includes four parts, i.e., Skyrme, symmetry, Coulomb, and Yukawa terms, which can be expressed as

$$U = \int H_{\text{Sky}} d\vec{r} + C_{\text{sym}} \frac{\rho_n - \rho_p}{\rho_0} \tau_z + \frac{1}{2}(1 - \tau_z)V_c + U_{\text{Yuk}}, \quad (3)$$

where $\rho_0 = 0.16 \text{ fm}^{-3}$ is the normal nuclear matter density, and ρ , ρ_n , and ρ_p are the total, neutron, and proton densities, respectively. τ_z is the z th component of the isospin degree of freedom, which equals 1 for neutrons or -1 for protons, respectively. $C_{\text{sym}} = 32 \text{ MeV}$ is the symmetry energy strength. V_c is the Coulomb potential. U_{Yuk} is the Yukawa potential, that is, surface potential. In particular, the Skyrme energy density can be parametrized by

$$H_{\text{Sky}} = \frac{\alpha}{2} \frac{\rho^2}{\rho_0} + \frac{\beta}{\gamma + 1} \frac{\rho^{\gamma+1}}{\rho_0^\gamma}. \quad (4)$$

The first term represents the two-body attractive interaction and the latter represents three-body repulsive interaction with three potential parameters, i.e., α , β , and γ , which determines the form of the nuclear EOS. In the model, $\alpha = -356 \text{ MeV}$, $\beta = 303 \text{ MeV}$, and $\gamma = 7/6$ are taken to represent the soft EOS without considering the momentum dependent potential. The fragments after freezing-out are constructed by the coalescence model [50,67–69] that the nucleons with the relative momentum smaller than $300 \text{ MeV}/c$ and the relative distance smaller than 3.5 fm are combined into a cluster.

The density distributions are given by the droplet model as in Refs. [41–43,70,71]. In the droplet model, the densities of neutrons and protons follow the Fermi distribution with two parameters, that is,

$$\rho_i(r) = \frac{\rho_i^0}{1 + \exp\left(\frac{r - C_i}{f_i t_i / 4.4}\right)}, \quad i = n, p, \quad (5)$$

where ρ_i^0 is the normalization constant ensuring that the density distribution equals to the number of neutrons ($i = n$) or protons ($i = p$), $C_i = R_i[1 - (0.413 f_i t_i / R_i)^2]$ is the half-density radius, t_i is the diffuseness parameter, and f_i is to adjust the diffuseness parameter which can give a good description of stable nuclei when it is equal to 1.0. Reference [12] found that C_i for a neutron and proton in heavy nuclei are almost the same, but t_i for the neutron is larger than that for the proton which determines the neutron-skin thickness. More details can be found in Refs. [72,73]. In order to obtain different sizes of neutron skin, we adjust f_n from 1.0 to 1.6, while maintaining $f_p = 1.0$ unchanged in this work. It can be found that for the neutron-rich nucleus, the density distribution of neutron is larger than that of the proton

and with the increase of f_n , the neutron density distribution is more extended and the neutron-skin thickness grows almost linearly.

In order to improve the self-consistency of the nuclear interaction potential used to determine the initial density distribution and evolution in the transport model, we can also obtain the density distribution by the SHF model which has been applied to a great variety of phenomena, including deformation properties, superheavy nuclei, vibrations, and heavy-ion collisions [74–79]. After continuous improvement, the widely used standard Skyrme energy density functions are obtained. Here, we mainly focus on the Skyrme two-body and three-body interaction which can be written in the following form:

$$H_{\text{SHF}} = \frac{t_0}{4} \left[2 + x_0 - (1 + 2x_0) \frac{1 + \delta^2}{2} \right] \rho^2 + \frac{t_3}{24} \left[2 + x_3 - (1 + 2x_3) \frac{1 + \delta^2}{2} \right] \rho^{\sigma+2}, \quad (6)$$

where $\delta = (\rho_n - \rho_p)/\rho$ is the isospin asymmetry and t_0 , t_3 , x_0 , x_3 , and σ are the Skyrme interaction parameters. Note that σ is also known as the density-dependent coefficient of the Skyrme interaction potential which commonly ranges from 1/6 to 1. When $\sigma < 1$, the potential is soft, while when $\sigma = 1$, the potential is stiff. So far, a great deal of Skyrme parameter sets have been proposed by fitting experimental data on some properties of nuclei and each set corresponds to its own macroscopic quantities, such as the nuclear symmetry energy at the saturation density, the slope of the symmetry energy, and the incompressibility of symmetric nuclear matter. A general review of Skyrme interaction and nuclear matter constraints can be found in Ref. [80]. Comparing Eq. (6) with Eq. (4), we can update the potential parameters (α , β , γ) in the IQMD model.

Our specific study procedures are as follows. First, we obtain neutron and proton density distributions of projectiles and targets by using the droplet model and acquire different values of S_n for projectiles by changing the factor f_n . Then we put the density distributions into the IQMD model as sampling functions to get the initial coordinate and momentum of each nucleon. In order to select the stable initialized nuclei, it is necessary to check their stability by the time evolution of the rms radii, neutron skin thickness, and binding energy until 200 fm/c. In the next step, the selected projectiles and targets are put into the IQMD model to simulate the collisions thus receiving detailed information on final fragments, such as the phase space, angular momentum, and binding energy. Based on the above data, subsequent analyses are conducted to investigate the correlations between the neutron-skin thickness and various physical quantities. For comparison, it was studied with the densities calculated by the SHF model instead of the droplet model. In this case, the same Skyrme parameters were used both in the SHF and IQMD model for consistency.

III. RESULTS AND DISCUSSION

By using the IQMD model, we simulate the semiperipheral collision processes of $^{44,47,60}\text{Ca}$, $^{28,32,37}\text{Mg}$, and $^{23,27,31}\text{Ne}$

with ^{12}C target at the incident energy of 50 MeV/nucleon. The reduced collision parameter \tilde{b} is defined as b/b_{max} to describe the colliding centrality, where the impact parameter b is the distance of the center of mass between the projectile and target, and the maximum impact parameter b_{max} is the sum of the rms radii of the projectile and target. Because the effect of neutron skin is mainly reflected on the surface of the nucleus, we focus on the semiperipheral collision with $0.6 < \tilde{b} < 1.0$ in our work. In addition, the rapidity of the fragments normalized to the incident projectile rapidity is defined as

$$\tilde{y} = \frac{1}{2} \ln \left(\frac{E + P_z}{E - P_z} \right) / y_{\text{proj}}, \quad (7)$$

where y_{proj} is the rapidity of the projectile, E is the total energy of the fragment, and P_z is the momentum of the fragment in the beam incidence direction. Particularly, all the above quantities are calculated in the center-of-mass system. We can use \tilde{y} to distinguish whether the fragment comes from the projectile or target and select the fragments with $\tilde{y} > 0$ to minimize the target effect. The dynamical process is simulated until 200 fm/c.

The difference of momentum between neutrons and protons [$\Delta P(n - p)$] is defined by the following expression:

$$\Delta P(n - p) = \frac{1}{N_n N_p} \sum_{i=1}^{N_n} \sum_{j=1}^{N_p} (|\vec{P}_{ni} - \vec{P}_{pj}|), \quad (8)$$

where N_n and N_p are total numbers of neutrons and protons. Figure 1 shows the time evolution of the momentum difference between neutrons and protons [$\Delta P(n - p)$] and the momentum difference between tritons and ^3He [$\Delta P(t - ^3\text{He})$] from 100 to 200 fm/c for ^{37}Mg on ^{12}C target at 50 MeV/nucleon under the condition of $0.6 < \tilde{b} < 1.0$ and $\tilde{y} > 0$. It can be seen that before 130 fm/c, all $\Delta P(n - p)$ and $\Delta P(t - ^3\text{He})$ drop rapidly. After that, $\Delta P(t - ^3\text{He})$ tends to be stable, while $\Delta P(n - p)$ decreases very slowly still keeping parallel and distinguishable with different neutron diffuseness parameters. We accumulate the emitted neutrons, protons, tritons, and ^3He between 170 fm/c and 200 fm/c to improve statistics. Consequently, the dependence of $\Delta P(n - p)$ on neutron-skin thickness is plotted in Fig. 2. Figure 2(a) illustrates the relationships for the nucleons of the initialized projectiles, while Figs. 2(b)–2(d) are for the emitted neutrons and protons after 170 fm/c. It indicates that no matter if in the initial or final state, there is a strong linear correlation between S_n and $\Delta P(n - p)$. $\Delta P(n - p)$ becomes smaller when S_n is larger. It means that if neutrons and protons get closer in space distribution, they will have larger difference in momentum distribution, which corresponds to the relationship between position and momentum as described in the uncertainty principle and representation transformation.

Figure 3 presents the dependence of $\Delta P(n - p)$ on the ratio of N to Z (N/Z) for Ca, Mg, and Ne isotopes in the final state with the same f_n . $f_n = 1.0$ refers to the neutron-skin thickness being predicted by the droplet model. It indicates that $\Delta P(n - p)$ is proportional to N/Z and a heavier nucleus results in a larger $\Delta P(n - p)$. Since it is relatively much easier

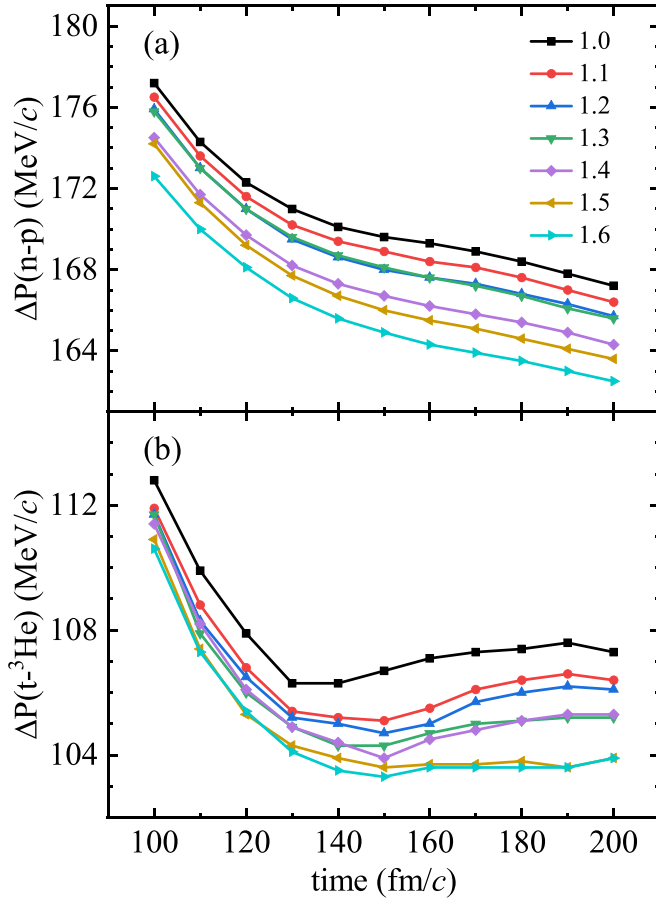


FIG. 1. Time evolution of $\Delta P(n-p)$ (a) and $\Delta P(t-{}^3\text{He})$ (b) for ${}^{37}\text{Mg} + {}^{12}\text{C}$ at 50 MeV/nucleon with $0.6 < \tilde{b} < 1.0$ and $\tilde{y} > 0$. Different colors correspond to different values of f_n .

to detect light charged particles in experiments, thus the dependence of $\Delta P(t-{}^3\text{He})$ on neutron-skin thickness is further studied. The correlation between S_n and $\Delta P(t-{}^3\text{He})$ in the final state becomes weak and the good linear relation exists only for very neutron-rich projectiles (${}^{60}\text{Ca}$, ${}^{37}\text{Mg}$, ${}^{31}\text{Ne}$) with large N/Z ($N/Z \approx 2$) as shown in Fig. 4. For the nucleus closer to the β -stability line, the probability of producing tritons and ${}^3\text{He}$ is lower causing the larger fluctuation. The value of $\Delta P(t-{}^3\text{He})$ is always smaller than the corresponding $\Delta P(n-p)$ for the same projectile. This may be due to the cancel-out effect between the three nucleons inside triton and ${}^3\text{He}$.

To see the effect of neutron-skin thickness on the momentum difference between neutrons and protons, a detailed study on momentum distributions of the emitted nucleons is carried out. With different f_n varying from 1.0 to 1.6, we systematically investigate the normalized momentum spectra of neutrons and protons at 200 fm/c without any condition on rapidity. It can be seen that the momentum spectra of neutrons are obviously different for different neutron-skin thicknesses, while those of protons are almost the same. The specific results under the conditions of $f_n = 1.0, 1.3, 1.6$ are taken as examples in Fig. 5(a). For quantitative comparison, the neutron momentum spectra are fitted by the Gaussian function.

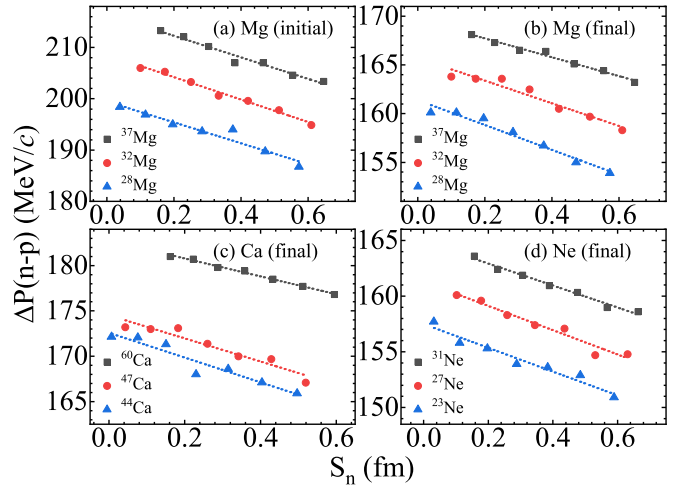


FIG. 2. Dependence of $\Delta P(n-p)$ on neutron-skin thickness for ${}^{28,32,37}\text{Mg} + {}^{12}\text{C}$ in the initial state (a), ${}^{28,32,37}\text{Mg} + {}^{12}\text{C}$ in the final state (b), ${}^{44,47,60}\text{Ca} + {}^{12}\text{C}$ in the final state (c), and ${}^{23,27,31}\text{Ne} + {}^{12}\text{C}$ in the final state (d) at 50 MeV/nucleon with $0.6 < \tilde{b} < 1.0$ and $\tilde{y} > 0$. The dotted lines are the results of linear fit.

The formula of Gaussian is given by

$$y = g_0 \exp \left[-\frac{1}{2} \left(\frac{x - g_1}{g_2} \right)^2 \right], \quad (9)$$

where the normalized constant g_0 is the peak height, the mean g_1 is the peak position, and the standard deviation g_2 is the full width at half-maximum (FWHM). Taking ${}^{37}\text{Mg}$ as an example, the dependence of the three fitting parameters on neutron-skin thickness is shown in Fig. 6. It is found that the peak becomes higher while the peak position and standard deviation become smaller with the neutron-skin thickness increasing. The same analysis is applied to other neutron-rich

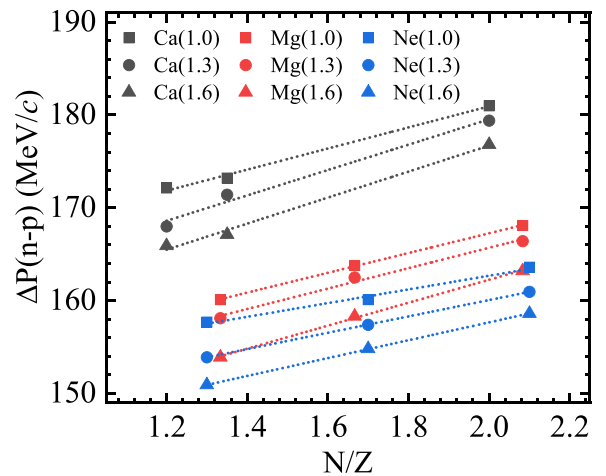


FIG. 3. Dependence of $\Delta P(n-p)$ on N/Z for ${}^{44,47,60}\text{Ca} + {}^{12}\text{C}$ (black), ${}^{28,32,37}\text{Mg} + {}^{12}\text{C}$ (red), and ${}^{23,27,31}\text{Ne} + {}^{12}\text{C}$ (blue) in the final state at 50 MeV/nucleon with $0.6 < \tilde{b} < 1.0$ and $\tilde{y} > 0$. Squares, circles, and triangles represent $f_n = 1.0, f_n = 1.3, f_n = 1.6$, respectively. The dotted lines are the results of linear fit.

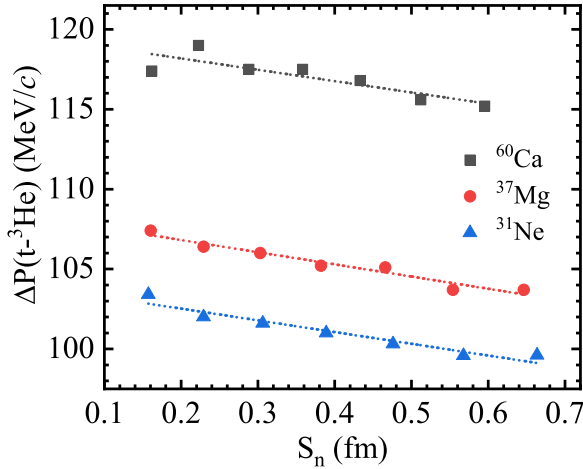


FIG. 4. Dependence of $\Delta P(t-{}^3\text{He})$ on neutron-skin thickness for ${}^{60}\text{Ca} + {}^{12}\text{C}$, ${}^{37}\text{Mg} + {}^{12}\text{C}$, and ${}^{31}\text{Ne} + {}^{12}\text{C}$ at 50 MeV/nucleon with $0.6 < \tilde{b} < 1.0$ and $\tilde{y} > 0$. The dotted lines are the results of linear fit.

projectiles. The peak position of the momentum distribution decreases linearly with the increase of the neutron-skin thickness. It indicates that the average momentum of neutrons produced in the final state becomes smaller. Since the average

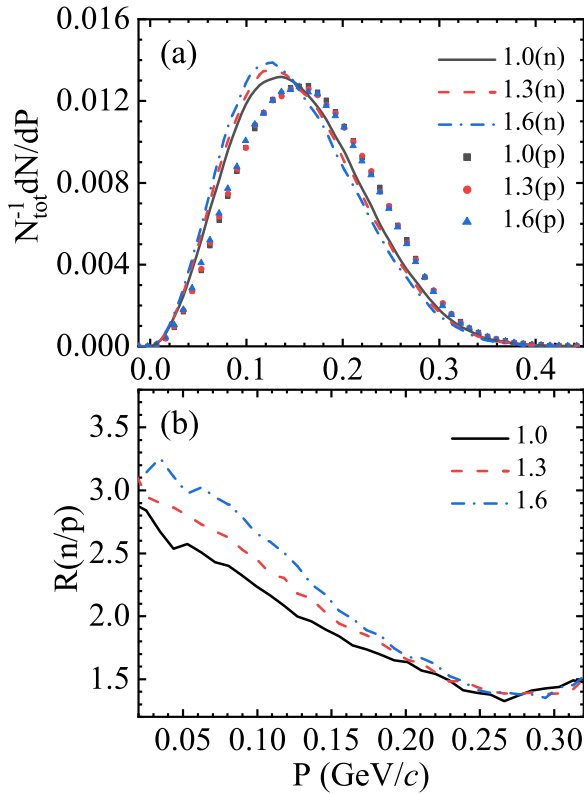


FIG. 5. The normalized momentum spectra of the emitted neutrons (shown by lines) and protons (shown by scatters) (a), and the momentum spectra of the ratio of neutrons to protons (b) at 200 fm/c for ${}^{37}\text{Mg} + {}^{12}\text{C}$ at 50 MeV/nucleon with $0.6 < \tilde{b} < 1.0$. Different symbols or line styles correspond to different values of f_n as shown in the legend.

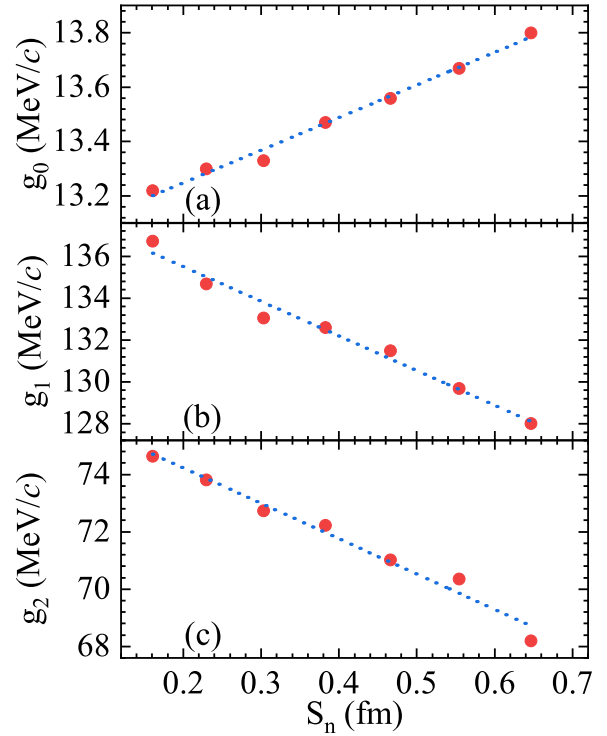


FIG. 6. Dependence of neutron momentum spectrum's Gaussian fitting parameters g_0 (a), g_1 (b), and g_2 (c) on neutron-skin thickness for ${}^{37}\text{Mg} + {}^{12}\text{C}$ at 50 MeV/nucleon with $0.6 < \tilde{b} < 1.0$. The dotted lines are the results of linear fit.

momentum of protons is constant, the momentum difference between neutrons and protons becomes smaller, which is in accordance with the above results between S_n and $\Delta P(n-p)$. According to the droplet model, the initial density distribution is more extended for neutrons while that of protons remains constant with increasing S_n . This anticorrelation between position and momentum satisfies the principles of quantum mechanics. More importantly, the yield ratio of neutrons to protons as a function of momentum is clearly dependent on the neutron-skin thickness by varying the diffuseness parameter and the cases of ${}^{37}\text{Mg}$ with $f_n = 1.0, 1.3$, and 1.6 are displayed in Fig. 5(b). It is evident that $R(n/p)$ is quite distinct from each other at small momentum for different neutron-skin sizes. With the increase of the momentum, the distinction gradually weakens and $R(n/p)$ tends to be consistent. Likewise, Ca and Ne isotope chains can give the same conclusion, confirming that the yield ratio of neutrons to protons at smaller momentum is more sensitive to the neutron-skin thickness than that at higher momentum. Therefore, we can select the neutrons and protons with a certain range of momentum, such as 0.07–0.13 GeV/c, to see the dependence of their yield ratio with the neutron-skin thickness. The results are in agreement with the conclusions in Ref. [49] obtained in the studies of peripheral collisions of ${}^{132}\text{Sn} + {}^{132}\text{Sn}$, ${}^{124}\text{Sn} + {}^{124}\text{Sn}$, and ${}^{112}\text{Sn} + {}^{112}\text{Sn}$ at 40 MeV/nucleon by using the IBUU model. They found that a larger symmetry energy could give a larger $R(n/p)$ and the effects of the symmetry potential are most prominent at lower kinetic energies. A large number of studies

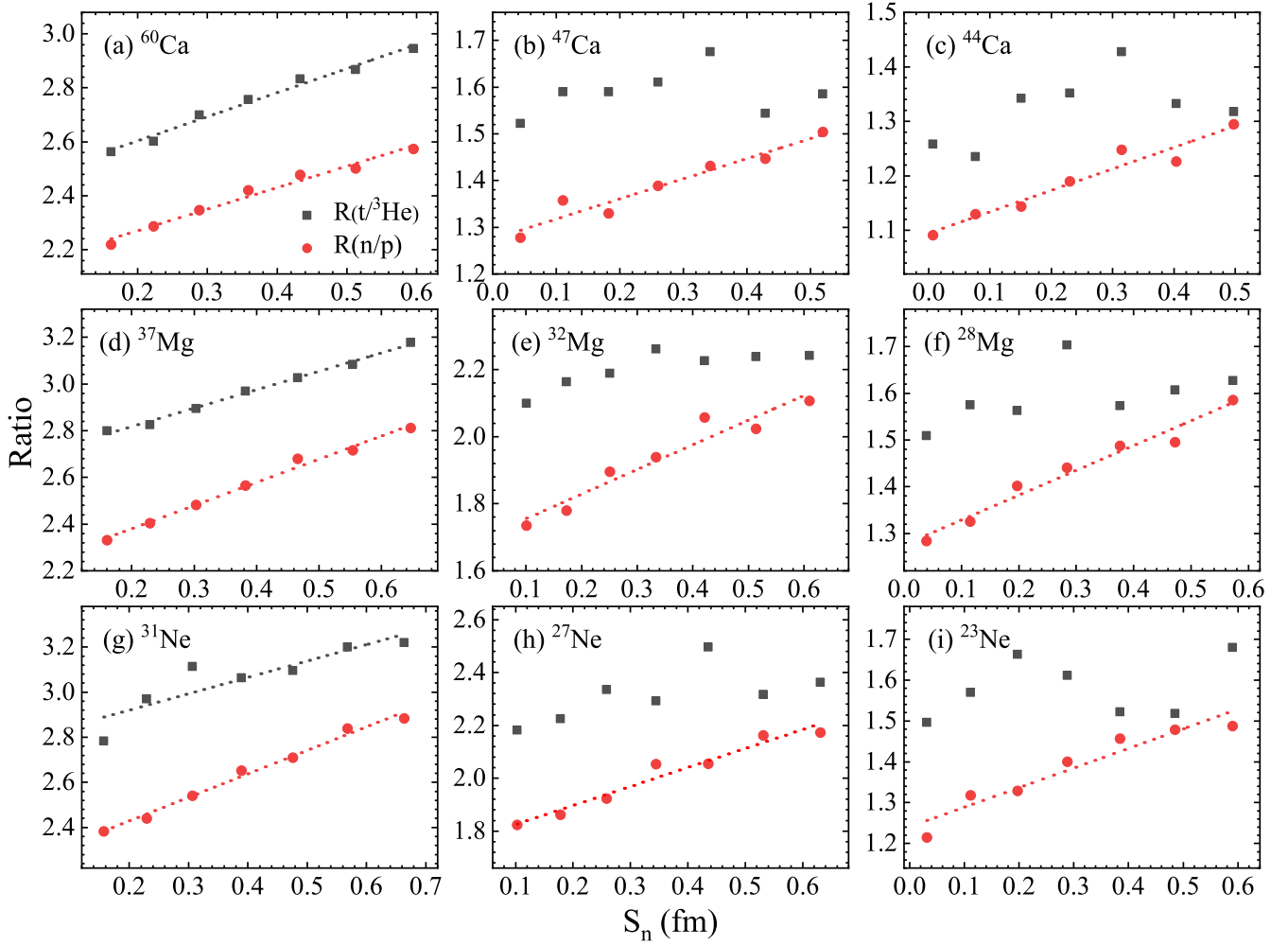


FIG. 7. Dependence of $R(n/p)$ and $R(t/{}^3\text{He})$ on neutron-skin thickness for ${}^{60}\text{Ca}$ (a), ${}^{47}\text{Ca}$ (b), ${}^{44}\text{Ca}$ (c), ${}^{37}\text{Mg}$ (d), ${}^{32}\text{Mg}$ (e), ${}^{28}\text{Mg}$ (f), ${}^{31}\text{Ne}$ (g), ${}^{27}\text{Ne}$ (h), and ${}^{23}\text{Ne}$ (i) on ${}^{12}\text{C}$ target at 50 MeV/nucleon with $0.6 < \bar{b} < 1.0$ and $\bar{y} > 0$. The dotted lines are the results of linear fit.

have suggested that there is a strong linear correlation between the neutron-skin thickness and symmetry energy, which is very clear and model-independent. As a result, with a thicker neutron skin, the symmetry potential is stronger so that more neutrons become unbound but they generally have smaller momentum.

Figure 7 displays the dependence of $R(n/p)$ and $R(t/{}^3\text{He})$ on neutron-skin thickness for ${}^{44,47,60}\text{Ca}$, ${}^{28,32,37}\text{Mg}$, and ${}^{23,27,31}\text{Ne}$ on a ${}^{12}\text{C}$ target with $\bar{y} > 0$. For different projectiles with different Z and N/Z , $R(n/p)$ is always directly proportional to S_n , which further confirms the results in Refs. [41,42]. Reference [43] found that $R(t/{}^3\text{He})$ could be a sensitive probe to extract S_n by simulating ${}^{50}\text{Ca} + {}^{12}\text{C}$ as well as ${}^{68}\text{Ni} + {}^{12}\text{C}$ and selecting the produced fragments with $\bar{y} > 0$. Specially, a notable phenomenon occurs on $R(t/{}^3\text{He})$ in this work that their strong linear dependence on S_n only appears in ${}^{60}\text{Ca}$, ${}^{37}\text{Mg}$, and ${}^{31}\text{Ne}$ with large N/Z and the correlation becomes weaker when the nucleus is closer to the β -stability line. The reason could be that the simulation result is no longer applicable when the neutron-skin thickness has a too large and unreasonable value.

Aiming to do a more self-consistent simulation in the IQMD, we replace the droplet model with the SHF model to obtain the initial density distribution for the projectile. By studying 240 sets of Skyrme parameters available in Ref. [80] with the SHF model, we ultimately select five parameter sets (Zs, SkSC1, BSk12, SkT3*, SkT4) to obtain different neutron-skin thicknesses. For the five parameter sets, their incompressibility coefficients are all around 230 MeV representing the soft EOS, while the slopes of the symmetry energy at the saturation density (L) are -29.38 MeV, 0.13 MeV, 38.01 MeV, 56.32 MeV, 93.49 MeV, respectively. In Fig. 8, we plot the proton and neutron density distributions of ${}^{37}\text{Mg}$ computed by the SHF model. The dependence of S_n with L is also presented in the inset. It can be found that, with the increase of L , the neutron density distribution is more extended and S_n is larger. The range of S_n is $0.3234\text{--}0.5387$ fm which is not as wide as that using the droplet model. Then these density distributions are used for the initialization and the same Skyrme potential parameters are used in the evolution and collision process in the IQMD model. Other conditions and analysis methods are the same as discussed above.

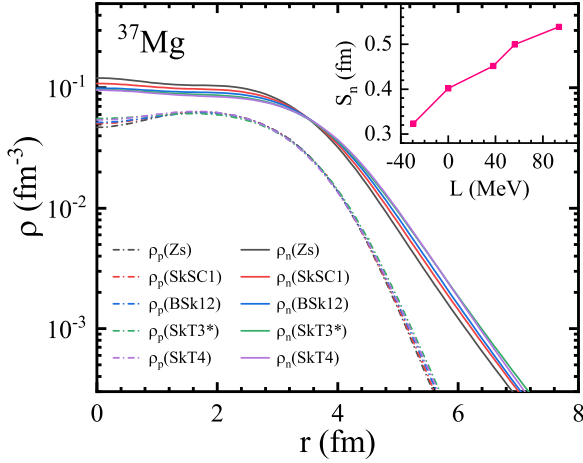


FIG. 8. The proton and neutron density distributions of ^{37}Mg computed from the SHF model. The correlation between L and S_n is in the inset plot.

Figure 9 illustrates the dependence of $R(n/p)$ and $R(t/{}^3\text{He})$ on neutron-skin thickness for $^{37}\text{Mg} + {}^{12}\text{C}$ and $^{31}\text{Ne} + {}^{12}\text{C}$ at 50 MeV/nucleon, and similar results are obtained.

From the above discussion, three probes are sensitive to the neutron-skin thickness for neutron-rich nuclei, i.e., the

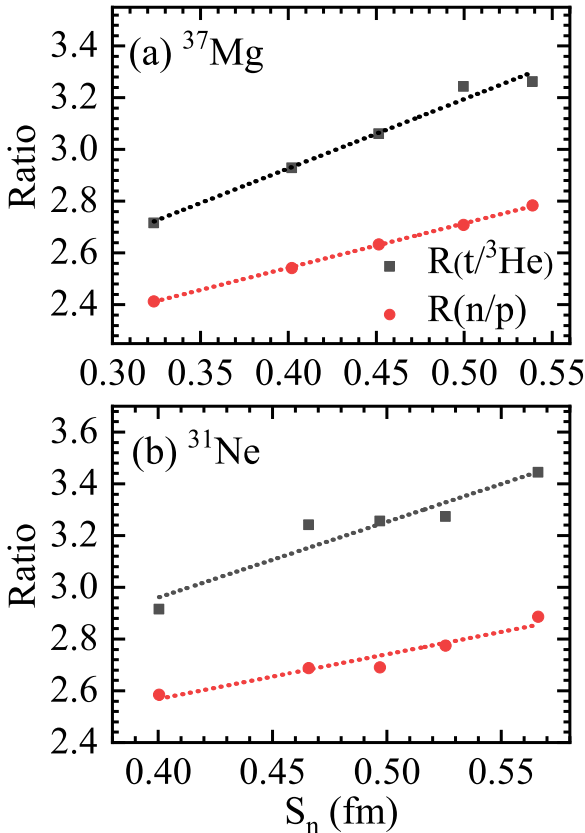


FIG. 9. Dependence of $R(n/p)$ and $R(t/{}^3\text{He})$ on neutron-skin thickness for ^{37}Mg (a) and ^{31}Ne (b) on ${}^{12}\text{C}$ target at 50 MeV/nucleon with $0.6 < \tilde{b} < 1.0$ and $\tilde{y} > 0$. The dotted lines are the results of linear fit.

difference of momentum between neutrons and protons, the peak position of the momentum spectrum of neutrons, and the yield ratio of neutrons to protons. As the neutron-skin thickness varying, these three quantities change by 3%, 8%, 19%, respectively, which implies the yield ratio is the most sensitive observable experimentally for neutron-skin thickness. With the development of the detector technology, the detection efficiency for neutron becomes large, thus making it feasible to extract useful information on the neutron-skin thickness from those proposed probes in future experiments. For example, the construction of the neutron wall for the external target experiment in the heavy-ion cooler-storage-ring project (HIRFL-CSR) at Lanzhou provides high efficiency for detecting neutrons. Furthermore, the similar simulations are also carried out in a more general energy region which is up to 150 MeV/nucleon. It is confirmed that even with different incident energies, strong correlations still exist between our proposed observables and the neutron-skin thickness. Our work mainly aims at the experiments in the HIRFL which will be performed at around 50 MeV/nucleon. For experiments at higher energies, the corresponding calculations can be done to give the theoretical support. Besides, through replacing ${}^{12}\text{C}$ with another nucleus as the target, such as ${}^9\text{Be}$, we find that the choice of the target nucleus will have little influence on the above conclusions.

IV. SUMMARY

Based on the IQMD model, the effects of neutron-skin thickness on light particles (neutron, proton, triton, and ${}^3\text{He}$) production from the reactions of ${}^{44,47,60}\text{Ca}$, ${}^{28,32,37}\text{Mg}$, and ${}^{23,27,31}\text{Ne}$ on a ${}^{12}\text{C}$ target at 50 MeV/nucleon under the condition of the reduced impact parameter from 0.6 to 1.0, i.e., semiperipheral collisions, have been systematically studied. For projectiles, different neutron-skin thicknesses are obtained by adjusting the neutron diffuseness parameter in the droplet model. The SHF model was also used to get the density distributions for comparison. The difference of momentum between neutrons and protons is defined as the average magnitude of the relative momentum in every possible permutation and combination. The dependence of $\Delta P(n-p)$ on the neutron-skin thickness is studied. It is obvious that both in the initial state and final state, $\Delta P(n-p)$ decreases linearly with the increase of S_n , which is in accordance with the uncertainty principle and representation transformation between coordinate and momentum space in quantum mechanics. The same analysis is performed for light charged particles, tritons, and ${}^3\text{He}$, which are easier to be measured experimentally compared with neutrons. It is suggested that the difference of momentum between tritons and ${}^3\text{He}$ could be used as a probe for the neutron-skin thickness of nuclei with large N/Z ($N/Z \approx 2$).

Further studies on momentum spectra at 200 fm/c indicate that the correlation between the peak position of neutrons and the neutron-skin thickness displays a similar linear trend which confirms the above results. Moreover, the yield ratio at small momentum for neutrons and protons is more sensitive to the neutron-skin thickness than that at large momentum. In addition, the yield ratio of neutrons to protons and the

yield ratio of tritons to ^3He are proportional to the neutron-skin thickness. Nevertheless, for the projectile closer to the β -stability line, the dependence of $R(t/{}^3\text{He})$ on the neutron-skin thickness becomes weak when the skin size is too large, indicating that the observables investigated in this work will be more feasible for the neutron-rich nuclei far from the β -stability line.

In conclusion, the difference of momentum between neutrons and protons, the peak position of the momentum spectrum of neutrons, and the yield ratios of neutrons to protons are sensitive to the neutron-skin thickness. And the effects of neutron-skin thickness on the production of tritons and ^3He exist mainly in very neutron-rich systems,

which are not as universal as those of neutrons and protons. These results can be important for extracting information of the neutron-skin thickness and the nuclear equation of state experimentally.

ACKNOWLEDGMENTS

This work is partially supported by the National Natural Science Foundation of China (Grants No. 11925502, No. 11935001, No. 12347106, No. 11961141003, No. 12147101, and No. 11890714), the Strategic Priority Research Program of Chinese Academy of Sciences (Grant No. XDB34030000), the National Key R&D Program of China (Grant No. 2023YFA1606404).

-
- [1] V. Baran, M. Colonna, V. Greco, and M. Di Toro, Reaction dynamics with exotic nuclei, *Phys. Rep.* **410**, 335 (2005).
- [2] B. Jonson, Light dripline nuclei, *Phys. Rep.* **389**, 1 (2004).
- [3] B. Blank and M. Borge, Nuclear structure at the proton drip line: Advances with nuclear decay studies, *Prog. Part. Nucl. Phys.* **60**, 403 (2008).
- [4] I. Tanihata, H. Savajols, and R. Kanungo, Recent experimental progress in nuclear halo structure studies, *Prog. Part. Nucl. Phys.* **68**, 215 (2013).
- [5] I. Angeli, A consistent set of nuclear rms charge radii: Properties of the radius surface $R(N,Z)$, *At. Data Nucl. Data Tables* **87**, 185 (2004).
- [6] G. W. Hoffmann, L. Ray, M. L. Barlett, R. Ferguson, J. McGill, E. C. Milner, K. K. Seth, D. Barlow, M. Bosko, S. Iverson, M. Kaletka, A. Saha, and D. Smith, Elastic scattering of 500-Mev polarized protons from $^{40,48}\text{Ca}$, ^{90}Zr , and ^{208}Pb , and breakdown of the impulse approximation at small momentum transfer, *Phys. Rev. Lett.* **47**, 1436 (1981).
- [7] V. E. Starodubsky and N. M. Hintz, Extraction of neutron densities from elastic proton scattering by $^{206,207,208}\text{Pb}$ at 650 Mev, *Phys. Rev. C* **49**, 2118 (1994).
- [8] A. Krasznahorkay, J. Bacelar, J. A. Bordewijk, S. Brandenburg, A. Buda, G. van 't Hof, M. A. Hofstee, S. Kato, T. D. Poelheken, S. Y. van der Werf, A. van der Woude, M. N. Harakeh, and N. Kalantar-Nayestanaki, Excitation of the isovector giant dipole resonance by inelastic α scattering and the neutron skin of nuclei, *Phys. Rev. Lett.* **66**, 1287 (1991).
- [9] G. Satchler, Isospin and macroscopic models for the excitation of giant resonances and other collective states, *Nucl. Phys. A* **472**, 215 (1987).
- [10] A. Krasznahorkay, M. Fujiwara, P. van Aarle, H. Akimune, I. Daito, H. Fujimura, Y. Fujita, M. N. Harakeh, T. Inomata, J. Jänecke, S. Nakayama, A. Tamii, M. Tanaka, H. Toyokawa, W. Uijen, and M. Yosoi, Excitation of isovector spin-dipole resonances and neutron skin of nuclei, *Phys. Rev. Lett.* **82**, 3216 (1999).
- [11] P. Lubiński, J. Jastrzębski, A. Trzcińska, W. Kurcewicz, F. J. Hartmann, W. Schmid, T. von Egidy, R. Smolańczuk, and S. Wycech, Composition of the nuclear periphery from antiproton absorption, *Phys. Rev. C* **57**, 2962 (1998).
- [12] A. Trzcińska, J. Jastrzębski, P. Lubiński, F. J. Hartmann, R. Schmidt, T. von Egidy, and B. Klos, Neutron density distributions deduced from antiprotonic atoms, *Phys. Rev. Lett.* **87**, 082501 (2001).
- [13] L. Ray, G. Hoffmann, and W. Coker, Nonrelativistic and relativistic descriptions of proton-nucleus scattering, *Phys. Rep.* **212**, 223 (1992).
- [14] B. A. Li, C. M. Ko, and W. Bauer, Isospin physics in heavy-ion collisions at intermediate energies, *Int. J. Mod. Phys. E* **07**, 147 (1998).
- [15] A. E. L. Dieperink, Y. Dewulf, D. Van Neck, M. Waroquier, and V. Rodin, Nuclear symmetry energy and the neutron skin in neutron-rich nuclei, *Phys. Rev. C* **68**, 064307 (2003).
- [16] J. Liu, C. Gao, N. Wan, and C. Xu, Basic quantities of the equation of state in isospin asymmetric nuclear matter, *Nucl. Sci. Tech.* **32**, 117 (2021).
- [17] J. M. Lattimer and M. Prakash, The physics of neutron stars, *Science* **304**, 536 (2004).
- [18] A. Steiner, M. Prakash, J. Lattimer, and P. Ellis, Isospin asymmetry in nuclei and neutron stars, *Phys. Rep.* **411**, 325 (2005).
- [19] B. A. Li, B. J. Cai, L. W. Chen, W. J. Xie, J. Xu, and N. B. Zhang, A theoretical overview of isospin and EOS effects in heavy-ion reactions at intermediate energies, *Nuovo Cim. C* **45**, 54 (2022).
- [20] L. Li, F. Y. Wang, and Y. X. Zhang, Isospin effects on intermediate mass fragments at intermediate energy-heavy ion collisions, *Nucl. Sci. Tech.* **33**, 58 (2022).
- [21] J. Xu, Constraining isovector nuclear interactions with giant dipole resonance and neutron skin in ^{208}Pb from a Bayesian approach, *Chin. Phys. Lett.* **38**, 042101 (2021).
- [22] Y. G. Ma, Hypernuclei as a laboratory to test hyperon-nucleon interactions, *Nucl. Sci. Tech.* **34**, 97 (2023).
- [23] P. C. Li, J. Steinheimer, T. Reichert, A. Kittiratpattana, M. Bleicher, and Q. F. Li, Effects of a phase transition on two-pion interferometry in heavy ion collisions at $\sqrt{s_{NN}} = 2.4\text{--}7.7\text{ GeV}$, *Sci. China Phys. Mech. Astron.* **66**, 232011 (2023).
- [24] C. M. Ko, Searching for QCD critical point with light nuclei, *Nucl. Sci. Tech.* **34**, 80 (2023).
- [25] G. F. Wei, X. Huang, Q. J. Zhi, A. J. Dong, C. G. Peng, and Z. W. Long, Effects of the momentum dependence of nuclear symmetry potential on pion observables in Sn+Sn collisions at 270 Mev/nucleon, *Nucl. Sci. Tech.* **33**, 163 (2022).
- [26] L. W. Chen, C. M. Ko, and B. A. Li, Nuclear matter symmetry energy and the neutron skin thickness of heavy nuclei, *Phys. Rev. C* **72**, 064309 (2005).
- [27] B. A. Brown, Neutron radii in nuclei and the neutron equation of state, *Phys. Rev. Lett.* **85**, 5296 (2000).

- [28] C. J. Horowitz and J. Piekarewicz, Neutron star structure and the neutron radius of ^{208}Pb , *Phys. Rev. Lett.* **86**, 5647 (2001).
- [29] C. J. Horowitz and J. Piekarewicz, Constraining Urca cooling of neutron stars from the neutron radius of ^{208}Pb , *Phys. Rev. C* **66**, 055803 (2002).
- [30] S. Typel and B. A. Brown, Neutron radii and the neutron equation of state in relativistic models, *Phys. Rev. C* **64**, 027302 (2001).
- [31] R. Furnstahl, Neutron radii in mean-field models, *Nucl. Phys. A* **706**, 85 (2002).
- [32] S. Karataglidis, K. Amos, B. A. Brown, and P. K. Deb, Discerning the neutron density distribution of ^{208}Pb from nucleon elastic scattering, *Phys. Rev. C* **65**, 044306 (2002).
- [33] M. Centelles, X. Roca-Maza, X. Viñas, and M. Warda, Nuclear symmetry energy probed by neutron skin thickness of nuclei, *Phys. Rev. Lett.* **102**, 122502 (2009).
- [34] H. L. Wei, X. Zhu, and C. Yuan, Configurational information entropy analysis of fragment mass cross distributions to determine the neutron skin thickness of projectile nuclei, *Nucl. Sci. Tech.* **33**, 111 (2022).
- [35] I. Vidaña, C. Providência, A. Polls, and A. Rios, Density dependence of the nuclear symmetry energy: A microscopic perspective, *Phys. Rev. C* **80**, 045806 (2009).
- [36] F. J. Fattoyev and J. Piekarewicz, Sensitivity of the moment of inertia of neutron stars to the equation of state of neutron-rich matter, *Phys. Rev. C* **82**, 025810 (2010).
- [37] F. J. Fattoyev and J. Piekarewicz, Neutron skins and neutron stars, *Phys. Rev. C* **86**, 015802 (2012).
- [38] X. Qu, H. Tong, C. Wang, and S. Wang, Neutron matter properties from relativistic Brueckner-Hartree-Fock theory in the full Dirac space, *Sci. China Phys. Mech. Astron.* **66**, 242011 (2023).
- [39] C. J. Jiang, Y. Qiang, D. W. Guan, Q. Z. Chai, C. Y. Qiao, and J. C. Pei, From finite nuclei to neutron stars: The essential role of high-order density dependence in effective forces, *Chin. Phys. Lett.* **38**, 052101 (2021).
- [40] W. J. Xie, Z. W. Ma, and J. H. Guo, Bayesian inference of the crust-core transition density via the neutron-star radius and neutron-skin thickness data, *Nucl. Sci. Tech.* **34**, 91 (2023).
- [41] X. Y. Sun, D. Q. Fang, Y. G. Ma, X. Z. Cai, J. G. Chen, W. Guo, W. D. Tian, and H. W. Wang, Neutron/proton ratio of nucleon emissions as a probe of neutron skin, *Phys. Lett. B* **682**, 396 (2010).
- [42] X. Y. Sun, D. Q. Fang, Y. G. Ma, X. Z. Cai, J. G. Chen, W. Guo, W. D. Tian, and H. W. Wang, A new probe of neutron skin thickness, *Chin. Phys. C* **35**, 555 (2011).
- [43] Z. T. Dai, D. Q. Fang, Y. G. Ma, X. G. Cao, and G. Q. Zhang, Triton/ ^3He ratio as an observable for neutron-skin thickness, *Phys. Rev. C* **89**, 014613 (2014).
- [44] T. Z. Yan and S. Li, Impact parameter dependence of the yield ratios of light particles as a probe of neutron skin, *Nucl. Sci. Tech.* **30**, 43 (2019).
- [45] T. Z. Yan and S. Li, Yield ratios of light particles as a probe of the proton skin of a nucleus and its centrality dependence, *Phys. Rev. C* **101**, 054601 (2020).
- [46] G. Bertsch and S. Das Gupta, A guide to microscopic models for intermediate energy heavy ion collisions, *Phys. Rep.* **160**, 189 (1988).
- [47] H. Wolter, M. Colonna, D. Cozma *et al.* (TMEP Collaboration), Transport model comparison studies of intermediate-energy heavy-ion collisions, *Prog. Part. Nucl. Phys.* **125**, 103962 (2022).
- [48] M. Colonna, Y. X. Zhang, Y. J. Wang, D. Cozma, P. Danielewicz, C. M. Ko, A. Ono, M. B. Tsang, R. Wang, H. Wolter, J. Xu, Z. Zhang, L. W. Chen, H. G. Cheng, H. Elfner, Z. Q. Feng, M. Kim, Y. Kim, S. Jeon, C. H. Lee *et al.*, Comparison of heavy-ion transport simulations: Mean-field dynamics in a box, *Phys. Rev. C* **104**, 024603 (2021).
- [49] B. A. Li, C. M. Ko, and Z. Z. Ren, Equation of state of asymmetric nuclear matter and collisions of neutron rich nuclei, *Phys. Rev. Lett.* **78**, 1644 (1997).
- [50] L. W. Chen, C. M. Ko, and B. A. Li, Light clusters production as a probe to nuclear symmetry energy, *Phys. Rev. C* **68**, 017601 (2003).
- [51] J. Aichelin, “Quantum” molecular dynamics—A dynamical microscopic n-body approach to investigate fragment formation and the nuclear equation of state in heavy ion collisions, *Phys. Rep.* **202**, 233 (1991).
- [52] Y. X. Zhang, N. Wang, Q. F. Li, L. Ou, J. L. Tian, M. Liu, K. Zhao, X. Z. Wu, and Z. X. Li, Progress of quantum molecular dynamics model and its applications in heavy ion collisions, *Front. Phys.* **15**, 54301 (2020).
- [53] J. Aichelin, G. Peilert, A. Bohnet, A. Rosenhauer, H. Stoecker, and W. Greiner, Quantum molecular dynamics approach to heavy ion collisions: Description of the model, comparison with fragmentation data, and the mechanism of fragment formation, *Phys. Rev. C* **37**, 2451 (1988).
- [54] Z. Q. Feng, Nuclear dynamics and particle production near threshold energies in heavy-ion collisions, *Nucl. Sci. Tech.* **29**, 40 (2018).
- [55] C. Liewen, Z. Fengshou, and J. Genming, Analysis of isospin dependence of nuclear collective flow in an isospin-dependent quantum molecular dynamics model, *Phys. Rev. C* **58**, 2283 (1998).
- [56] X. G. Cao, X. Z. Cai, Y. G. Ma, D. Q. Fang, G. Q. Zhang, W. Guo, J. G. Chen, and J. S. Wang, Nucleon-nucleon momentum-correlation function as a probe of the density distribution of valence neutrons in neutron-rich nuclei, *Phys. Rev. C* **86**, 044620 (2012).
- [57] J. Y. Liu, W. J. Guo, Z. Z. Ren, Y. Z. Xing, W. Zuo, and X. G. Lee, Special roles of loose neutron-halo nucleus structure on the fragmentation and momentum dissipation in heavy ion collisions, *Phys. Lett. B* **617**, 24 (2005).
- [58] C. Tao, Y. G. Ma, G. Q. Zhang, X. G. Cao, D. Q. Fang, and H. W. Wang, Pygmy and giant dipole resonances by Coulomb excitation using a quantum molecular dynamics model, *Phys. Rev. C* **87**, 014621 (2013).
- [59] Y. G. Ma and W. Q. Shen, Onset of multifragmentation in intermediate energy light asymmetrical collisions, *Phys. Rev. C* **51**, 710 (1995).
- [60] F. S. Zhang, L. W. Chen, Z. Y. Ming, and Z. Y. Zhu, Isospin dependence of nuclear multifragmentation in $^{112}\text{Sn} + ^{112}\text{Sn}$ and $^{124}\text{Sn} + ^{124}\text{Sn}$ collisions at 40 MeV/nucleon, *Phys. Rev. C* **60**, 064604 (1999).
- [61] Y. G. Ma, Y. B. Wei, W. Q. Shen, X. Z. Cai, J. G. Chen, J. H. Chen, D. Q. Fang, W. Guo, C. W. Ma, G. L. Ma, Q. M. Su, W. D. Tian, K. Wang, T. Z. Yan, C. Zhong, and J. X. Zuo, Surveying the nucleon-nucleon momentum correlation function in the framework of quantum molecular dynamics model, *Phys. Rev. C* **73**, 014604 (2006).
- [62] Y. G. Ma and W. Q. Shen, Correlation functions and the disappearance of rotational collective motion in nucleus-nucleus

- collisions below 100 MeV/nucleon, *Phys. Rev. C* **51**, 3256 (1995).
- [63] C. Liu, X. G. Deng, and Y. G. Ma, Density fluctuations in intermediate-energy heavy-ion collisions, *Nucl. Sci. Tech.* **33**, 52 (2022).
- [64] C. Hartnack, R. K. Puri, J. Aichelin, J. Konopka, S. A. Bass, H. Stöcker, and W. Greiner, Modelling the many-body dynamics of heavy ion collisions: Present status and future perspective, *Eur. Phys. J. A* **1**, 151 (1998).
- [65] S. Gautam, R. Chugh, A. D. Sood, R. K. Puri, C. Hartnack, and J. Aichelin, Isospin effects on the energy of vanishing flow in heavy-ion collisions, *J. Phys. G* **37**, 085102 (2010).
- [66] N. Wang, Z. Li, and X. Wu, Improved quantum molecular dynamics model and its applications to fusion reaction near barrier, *Phys. Rev. C* **65**, 064608 (2002).
- [67] J. Singh and R. K. Puri, Dynamical multifragmentation and spatial correlations, *Phys. Rev. C* **62**, 054602 (2000).
- [68] S. Goyal and R. K. Puri, Formation of fragments in heavy-ion collisions using a modified clusterization method, *Phys. Rev. C* **83**, 047601 (2011).
- [69] S. Kumar and Y. Ma, Directed flow of isospin sensitive fragments within a modified clusterization algorithm in heavy-ion collisions, *Nucl. Sci. Tech.* **24**, 50509 (2013).
- [70] Z. T. Dai, D. Q. Fang, Y. G. Ma, X. G. Cao, G. Q. Zhang, and W. Q. Shen, Effect of neutron skin thickness on projectile fragmentation, *Phys. Rev. C* **91**, 034618 (2015).
- [71] S. S. Wang, Y. G. Ma, D. Q. Fang, and X. G. Cao, Effects of neutron-skin thickness on direct hard photon emission from reactions induced by the neutron-rich projectile ^{50}Ca , *Phys. Rev. C* **105**, 034616 (2022).
- [72] W. Myers and W. Swiatecki, Droplet-model theory of the neutron skin, *Nucl. Phys. A* **336**, 267 (1980).
- [73] W. D. Myers and K. H. Schmidt, An update on droplet-model charge distributions, *Nucl. Phys. A* **410**, 61 (1983).
- [74] K. Langanke, J. A. Maruhn, and S. E. Koonin, *Computational Nuclear Physics I: Nuclear Structure* (Springer, Berlin/Heidelberg, 1991).
- [75] P. Quentin and H. Flocard, Self-consistent calculations of nuclear properties with phenomenological effective forces, *Annu. Rev. Nucl. Part. Sci.* **28**, 523 (1978).
- [76] K. Goeke, R. Y. Cusson, F. Grümmer, P. G. Reinhard, and H. Reinhardt, Time dependent Hartree-Fock and beyond, *Prog. Theor. Phys. Suppl.* **74**, 33 (1983).
- [77] E. Chabanat, P. Bonche, P. Haensel, J. Meyer, and R. Schaeffer, A Skyrme parametrization from subnuclear to neutron star densities, *Nucl. Phys. A* **627**, 710 (1997).
- [78] J. Friedrich and P. Reinhard, Skyrme-force parametrization: Least-squares fit to nuclear ground-state properties, *Phys. Rev. C* **33**, 335 (1986).
- [79] P. Klüpfel, P.-G. Reinhard, T. J. Bürvenich, and J. A. Maruhn, Variations on a theme by Skyrme: A systematic study of adjustments of model parameters, *Phys. Rev. C* **79**, 034310 (2009).
- [80] M. Dutra, O. Lourenço, J. S. Sá Martins, A. Delfino, J. R. Stone, and P. D. Stevenson, Skyrme interaction and nuclear matter constraints, *Phys. Rev. C* **85**, 035201 (2012).